SAND2022-11153C

Design and fabrication of multi-metal patterned target anodes for improved quality of hyperspectral X-ray radiography and computed tomography imaging systems

Courtney L. Hummell[a], Noelle M. Collins[b], Gabriella M. Dalton[b], Rebecca A. Wheeling[c], Jeier Yang[c], Kyle R. Thompson[b], Ray S. Fuentes[d], and Edward S. Jimenez[b]

[a]Sandia National Laboratories, III-V Optoelectronics & HI, Albuquerque, NM, USA
[b]Sandia National Laboratories, Non-destructive Evaluation & Diagnostic Development, Albuquerque, NM, USA
[c]Sandia National Laboratories, Metallurgy and Materials Joining, Albuquerque, NM, USA
[d]Sandia National Laboratories, Materials Reliability, Albuquerque, NM, USA

ABSTRACT

Applications such as counterfeit identification, quality control, and non-destructive material identification benefit from improved spatial and compositional analysis. X-ray Computed Tomography is used in these applications but is limited by the X-ray focal spot size and the lack of energy-resolved data. Recently developed hyperspectral X-ray detectors estimate photon energy, which enables composition analysis but lacks spatial resolution. Moving beyond bulk homogeneous transmission anodes toward multi-metal patterned anodes enables improvements in spatial resolution and signal-to-noise ratios in these hyperspectral X-ray imaging systems. We aim to design and fabricate transmission anodes that facilitate confirmation of previous simulation results. These anodes are fabricated on diamond substrates with conventional photolithography and metal deposition processes. The final transmission anode design consists of a cluster of three disjoint metal bumps selected from molybdenum, silver, samarium, tungsten, and gold. These metals are chosen for their k-lines, which are positioned within distinct energy intervals of interest and are readily available in standard clean rooms. The diamond substrate is chosen for its high thermal conductivity and high transmittance of X-rays. The feature size of the metal bumps is chosen such that the cluster is smaller than the 100 µm diameter of the impinging electron beam in the X-ray tube. This effectively shrinks the X-ray focal spot in the selected energy bands. Once fabricated, our transmission anode is packaged in a stainless-steel holder that can be retrofitted into our existing X-ray tube. Innovations in anode design enable an inexpensive and simple method to improve existing X-ray imaging systems.

Keywords: Hyperspectral X-ray, Resolution, Fabrication, Anode, Computer Tomography, Photolithography, Material Identification, Simulation Validation

1. INTRODUCTION

Hyperspectral Computed Tomography (H-CT) is an advanced nondestructive evaluation technique that adds the ability to determine material composition via energy discriminated information. In traditional CT, each pixel of the detector yields a single integrated intensity value and is not useful for elemental analysis. Additionally, the intensity value is defined by a nonlinear mathematical operator due to the wide variation of attenuation values for a given material, which results in degraded image quality due to beam-hardening artifacts.[1] In H-CT, for each pixel, incident photons are counted and binned into discrete channels according to their energy. This enhances the ability to distinguish between the elements contained in a sample.[1] The spatial resolution of both CT and H-CT systems are limited by both the focal spot size of the electron beam impinging on the anode and the detector's physical pixel size. H-CT systems require semiconductor detectors, while traditional CT systems use either semiconductor or scintillation-based detectors, which generally have reduced pixel sizes. Moreover,

Further author information: (Send correspondence to Edward Jimenez)
Edward Jimenez: E-mail: esjimen@sandia.gov , Telephone: 1 505 284-9690

H-CT systems require longer acquisition times to ensure sufficient photon counts in each energy channel as well as to avoid pulse pile-up from photon saturation which is problematic for some applications.[2]

The spectral information acquired by an H-CT system can be bandpassed to reconstruct narrow spectral neighborhoods. Constraining the spectral width effectively linearizes the mathematical operator that defines the imaging system by indirectly limiting the range of attenuation values for a given material, consequently improving image quality by reducing beam-hardening artifacts. Additionally, image quality is improved by targeting spectral neighborhoods about the characteristic peaks, as these spectral neighborhoods are areas of increased photon flux and thus increased signal-to-noise ratio (SNR).[3]

In pursuit of both spectral and spatial resolution improvements, we designed two versions of a custom multi-metal anode that can be easily integrated with an existing commercial-off-the-shelf microfocus X-ray tube with replaceable anodes. The proposed custom anodes improve image quality by increasing SNR in spectral neighborhoods corresponding to the characteristic emission peaks of multiple materials within a single anode. In addition, the multi-metal anode's target materials are patterned to effectively shrink the focal spot size, thus improving spatial resolution.

Both custom anode designs consist of several candidate metals. The resulting spectrum from these anodes contain multiple characteristic emission peaks, which are areas of high SNR. The first design is a reflection anode that is composed of two metals layered in bulk onto the surface of a commercially available tungsten (W) reflection anode. The second design is for a transmission anode containing three candidate metals patterned into cylindrical features in clusters smaller than the focal spot size of the electron beam. Using these smaller feature sizes improves spatial resolution over conventional bulk W anodes while simultaneously taking advantage of the range of emission energies from multiple materials. Moreover, this patterned anode is made using standard photolithography processes and is readily integrated into an existing X-ray tube. Thus, the fabrication method for the patterned anode is practical and easily repeatable, as well as customizable by any facility with a standard cleanroom.

2. BACKGROUND

2.1 Hyperspectral Computed Tomography

The H-CT system featured in this work is comprised of an X-ray source manufactured by X-RAY WorX with a Cadmium-Telluride (Cd-Te) detector manufactured by Detection Technologies. The X-ray source has a maximum accelerating voltage capacity of 225 keV. The detector is 0.5 meters wide and is composed of a linear array of 640 energy-discriminating pixels calibrated to a maximum energy of 160 keV across 128 energy channels. The detector produces spectral data, such that when a photon interacts with a pixel on the detector, the photon is binned into one of 128 channels based on its energy. The spatial resolution improvements described in this work are inspired of the previous work of Zhou et al.[4] They proposed that using an anode comprised of a substrate transparent to X-rays with embedded metal features smaller than the electron beam effectively shrinks the focal spot size of the system to the size of the smaller metal features. Zhou et al.[4] demonstrated this through simulation, showing that the X-rays generated from the anode mostly come from the embedded metal features while radiation generated from the substrate was minimal. This established that the effective focal spot size is proportional to the diameter of the metal in the anode, thus improving spatial resolution.

The X-RAY WorX system allows reduction of the effective focal spot size by reducing X-ray tube current at a constant energy. However, this alteration limits the photon flux and increases acquisition times. Alternatively, decreasing tube voltage could also reduce the focal spot size; however, this constrains the X-ray penetration ability, which reduces the ability to image materials composed of heavy elements and limits imaging thicker or higher density materials. This spatial resolution compared to photon flux tradeoff is similarly seen in Talbot–Lau grating-based X-ray phase contrast imaging (XPCI).[5] In XPCI, the Talbot–Lau grating configuration consists of three gratings; many photons are lost through absorption in these gratings. Morimoto et al. experimentally demonstrated that the source and absorption gratings can be replaced by using a transmission anode containing a single-metal-multi-dot array embedded in a diamond substrate. This combined with a phase grating creates spatially coherent X-ray emission. This configuration resulted in producing XPCI images more efficiently and with fewer artifacts.[5]

Previous work by Dalton et al.[6] showed through simulation that a multi-metal patterned anode based on the combined efforts by Zhou et al.[4] and Morimoto et al.[5] and combined with a hyperspectral X-ray detector further improves spatial resolution when focused on narrow X-ray energy neighborhoods. This work simulated a typical W anode and a multi-metal patterned anode; the goal of the simulations was to compare SNR and spatial resolution about the emission lines of the metals contained within the multi-metal anode. Through simulated X-ray images of duplex wire line-pair gauges of various wire diameters, it was shown that the multi-metal anode consistently exhibited superior spatial resolution compared to the traditional W anode for each magnification simulated. Furthermore, this work also demonstrated that a multi-metal patterned anode combined with a hyperspectral X-ray detector improves SNR appreciably at energy ranges corresponding to the characteristic peaks of the materials present in the anode.

3. METHODS AND DESIGN

3.1 Material Selection

3.1.1 Substrates

Multi-crystalline diamond grown by chemical vapor deposition (CVD) was selected as the substrate for the anode fabrication for its X-ray transparency as well as its high thermal conductivity. The heat generated by the impinging electron beam and X-ray generation must be spread through the diamond substrate and diffused into the stainless steel (SS) holder and X-ray tool to avoid thermally melting or damaging the active layer metals. CVD-diamond substrates with specified thermal conductivity, T_c $>1000\,\mathrm{W\,m^{-1}\,K^{-1}}$ were purchased from Mintres. The dimensions were matched to the substrates used in the commercially available X-RAY WorX High Energy transmission anodes for sake of achieving comparable thermal load and performance: $12\,\mathrm{mm} \pm 0.05$ diameter and $0.27\,\mathrm{mm} \pm 0.03$ thick.

3.1.2 Candidate Anode Metals

X-ray anode materials tend to be selected for their high melting point, which withstands heating from the high electron flux needed to yield high emission signal. Further, high atomic number (Z) and corresponding high atomic electron density result in more efficient X-ray generation by the impinging electrons from the cathode. High density also corresponds to improved heat conduction away from the focal spot to diffuse into the rest of the anode.

However, it may be desired to select anode materials with more intermediate Z numbers such as molybdenum (Mo) or silver (Ag) for imaging of soft tissue or other lower density samples.[7] For these reasons, W and gold (Au) are commonly used for high energy sources while Ag and Mo are more typical for low energy sources and applications. Samarium (Sm) is less common, but can serve similar applications to Ag and Mo and approaches more intermediate energy bands between those and W. Ytterbium (Yb) similarly could provide an intermediate energy band between Sm and W.

In addition to the high-count signals for the K_α emissions, the K_β peaks as well as secondary X-ray generation must be considered. Secondary X-ray generation can include interactions amongst anode materials when multiple are included as well as from the anode X-rays interacting with the photodetector materials. For example, a $K_{\alpha 1}$ X-ray emitted from Au may interact with a Sm atom and result in a Sm $K_{\alpha 1}$ emission. In doing so, the original X-ray loses energy and would have a new energy of approximately $K_{\alpha 1,Au}$-$K_{\alpha 1,Sm}$, or 28.7 keV. This secondary X-ray emission is near in energy to the Ag, Cd, and Te $K_{\alpha 1}$ and would be counted in the same spectral neighborhood as the Ag and detector peaks rather than the neighborhood of the Au peak.

Important characteristic density, melting point, and emission energy values are listed for the candidate metals of interest and our detector components, Cd and Te, in Table 1. The characteristic emission energies for the selected materials are also plotted in Fig. 1.

While there are other suitable anode materials, each of the candidate metals listed here are available for deposition in Sandia's Microsystems Engineering Science and Applications (MESA) Microfab, apart from Uranium (U), and the collection of them spans a broad range of characteristic X-ray energies. Uranium is included as a potential candidate for the highest energy emission lines available but has a variety of complications for implementation.

Table 1. Characteristic X-ray emission energies and material properties of the candidate metals of interest. X-ray data from Table 1-2 of the 3rd edition of Lawrence Berkeley National Laboratories' *X-ray Data Booklet*[8]

Element	Z number	Melting Point (°C)	Density ($\frac{g}{cm^3}$)	$K_{\alpha 1}$ (keV)	$K_{\alpha 2}$(keV)	$K_{\beta 1}$ (keV)
Ti	22	1660	4.5	4.51	4.50	4.93
Mo	42	2610	10.22	17.48	17.37	19.61
Ag	47	962	10.5	22.16	21.99	24.94
Cd	48	321	8.65	23.17	22.98	26.10
Te	52	452	6.25	27.47	27.20	31.00
Sm	62	1072	7.52	40.12	39.52	45.41
Yb	70	819	6.97	52.39	51.35	59.37
W	74	3410	19.3	59.32	57.98	67.24
Au	79	1064	19.3	68.80	66.99	77.98
U	92	1132	19.1	98.44	94.67	111.30

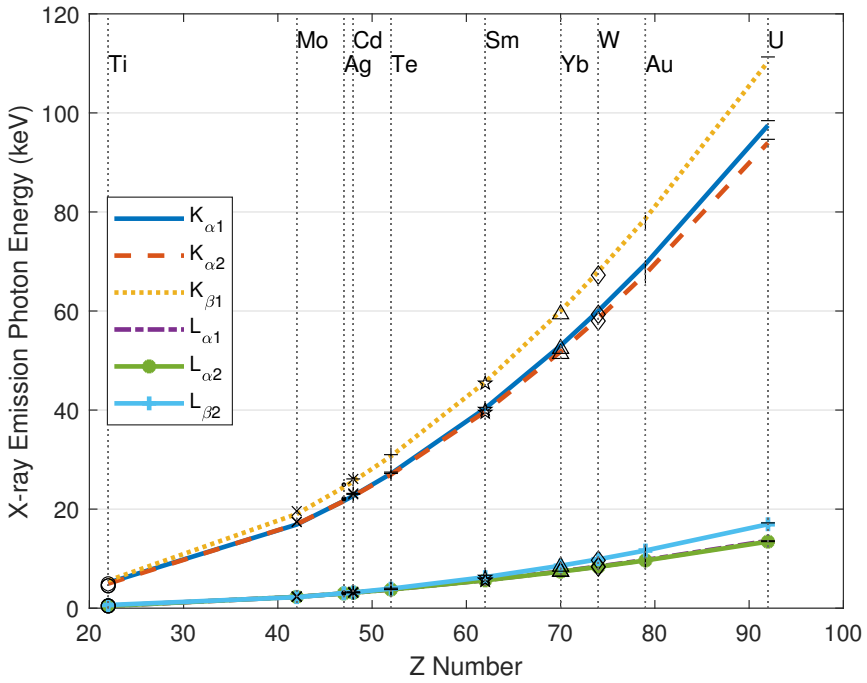

Figure 1. Characteristic X-ray emission energies of the candidate metals of interest and the Cd Te detector. X-ray data from Table 1-2 of the 3rd edition of Lawrence Berkeley National Laboratories' *X-ray Data Booklet*[8]

Mo was one of the metals selected in Dalton et al.'s[6] simulation, but is a difficult material to deposit as a film of appreciable thickness without thorough development. It does not sublimate from solid state and must be melted, but the melting point of 2623 °C causes rapid heating of the chamber and substrate. Lengthy deposition time and the subsequent >250 °C rise in chamber temperature for 0.5 µm film thickness resulted in film cracking and delamination upon removal from the evaporation chamber. It was abandoned as a material candidate after initial development failure.

3.2 Reflection Anode

Reflection anodes are post-style anodes with angled metal surfaces on the head. Electrons strike the angled anode surface and generate X-rays that are emitted isotropically. The X-rays that are not self-absorbed in the anode travel towards the object being imaged. The key consideration for the layered design is accounting for differences in density between the selected metals with respect to X-ray emission propagation. The X-rays can be scattered or absorbed along the way from their generation points burried within the anode stack and as such, the order of the metal layering should have the highest density deepest in the anode, as in nearest the center, and the lowest density at the surface. A commercial X-RAY WorX reflection anode with a bulk W cap is used as the base, and should have the next highest density material deposited followed by the lowest density to help minimize X-ray scattering and absorption. The original design was to be 5000 Å each of W-Mo-Ag, but due to the Mo deposition complications described in Sec. 3.1.2, adjustments were made and W-Au-Ag was used instead. As with the transmission anodes, thin 20 Å titanium (Ti) layers were included to facilitate adhesion between the metals of interest.

3.3 Transmission Anode

3.3.1 Patterned Transmission Anode

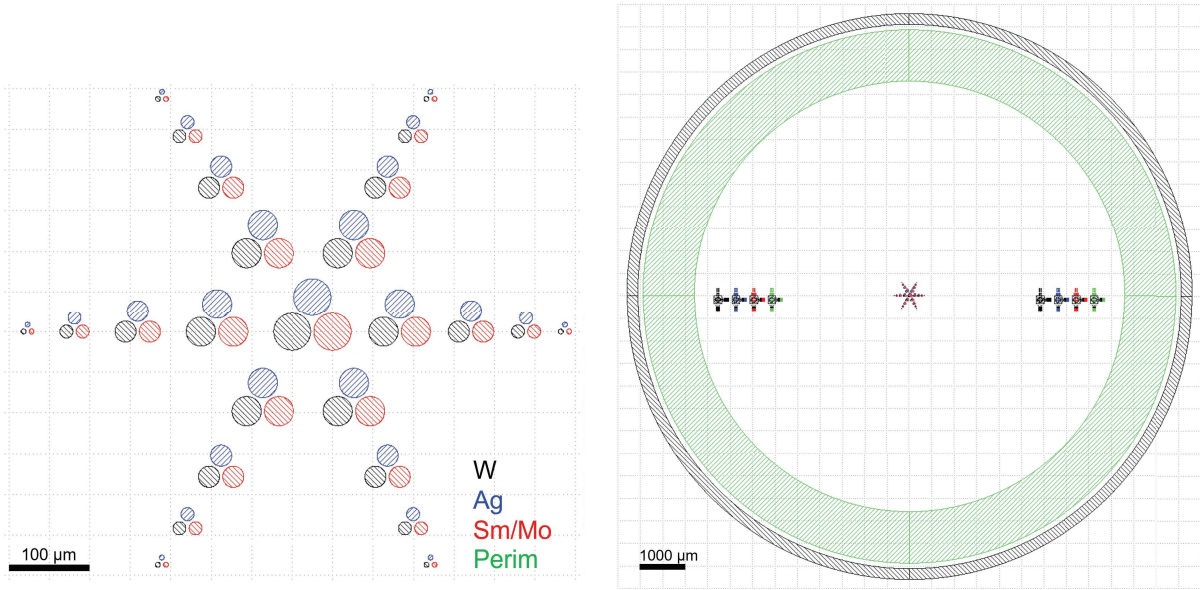

Figure 2. Left) "Cluster Trio" array in the middle 700 µm of the photolithography masks. Right) The full mask, with alignment marks in the outer 7 mm of the substrate and an outer perimeter layer for plating the outer 30 % of the substrate.

The patterned design for the transmission anode is acheived via contact photolithography. The photolithography masks were written in MATLAB using the GDSII-Toolbox developed by Ulf Griesmann of NIST.[9] Based on Dalton et al.'s[6] simulation work mentioned previously, the masks were drawn to include an array of "cluster trios" of varying diameters. The clusters, shown in Fig. 2 range from around 16 µm to 100 µm in diameter, to fit within the 100 µm focal spot size of the X-ray system. The largest cluster of 100 µm is centered in the mask as it most likely to yield a high signal. The electron beam can can be steered resulting in movement of the focal spot as anode materials wear out, so the clusters are spread out radially with a 100 µm pitch but are only present in the center 700 µm of the wafer within beam steerability. There is a mask for each of the three candidate metals of interest in the cluster, plus a perimeter layer for adding seed metal and electroplating before soldering. The candidate metal layers are offset from one another by 4 µm to account for fabrication tolerance.

3.3.2 Layered Transmission Anode

In addition to the patterned anode fabrication, simple layered, bulk anodes were designed for initial emission-spectra characterization to compare with the reflection anodes. These will be used to characterize the benefits of the inclusion of multiple anode materials without obfuscation by the anticipated signal reduction correlated to focal spot size reduction. For the transmission anodes, the candidate metal layers must be in order from the lowest density at the substrate to the highest density metal at the top surface. This is to prevent excessive scattering or absorption of the surface-generated X-rays by the deeper materials as the X-rays transmit through the stack and then substrate before reaching the sample. Two versions of the layered anodes were designed, one using a transmission anode design and the other using a reflection anode.

The layered transmission anodes effectively match the patterned transmission anodes except they do not use photolithography. In the case of our fabrication, the lowest density metal, Sm, is deposited onto the prepared diamond substrate first, followed by Ag and finishing with W or Au. Thin 20 Å to 100 Å layers of Ti are included in between the 5000 Å candidate metals to facilitate adhesion, but the thinness and low density compared to the metals of interest should prevent significant additional scattering or absorption.

3.4 Transmission Anode Packaging

3.4.1 Holders

Design of the holders was constrained by parameters for mounting into our existing X-RAY WorX X-ray tube. We matched the X-RAY WorX High Energy anode dimensions in SolidWorks as shown in Fig. 3 and had them machined from SS 1.4305.

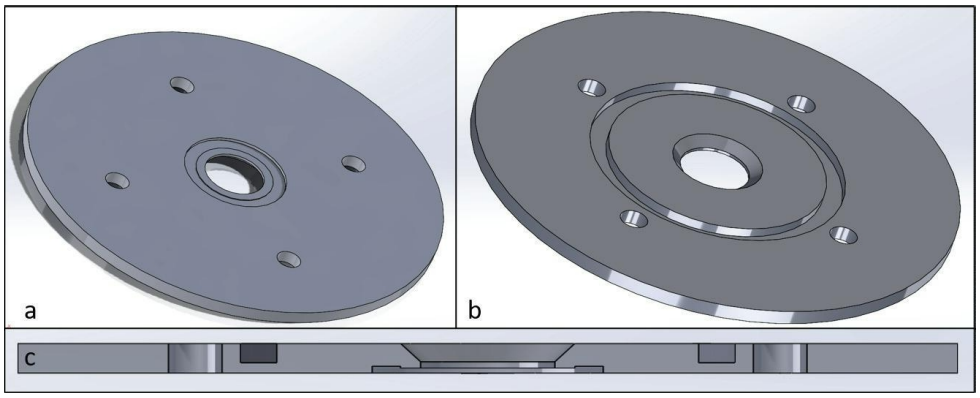

Figure 3. SolidWorks drawings of a) back, b) front, and c) cross section view of our custom transmission anode packaging.

3.4.2 Assembly

Once the transmission anode substrates are fabricated, they must be soldered into the holders to mount onto the X-ray tube. The SS holders were electroplated with 4 µm to 5 µm of nickel (Ni) followed by 2 µm of Au. The plated substrates are soldered into the holders to achieve a vacuum-tight seal. $Sn_{63}Pb_{37}$ preforms were purchased from Indium Corporation with dimensions chosen to most closely match to the channel machined in the SS holders, with an inner diameter of 0.398″, outer diameter of 0.478″, and thickness of 0.02″.

The $Sn_{63}Pb_{37}$ preforms and the patterned diamond substrates were clamped with Nalgene polypropylene forceps for easier handling and to prevent scratches during the cleaning process. The preforms, substrates, and SS holders were ultrasonically rinsed in degreasing solvent (Aerotron-100^{TM}) and subsequently in isopropanol (IPA) for 2 minutes each and air dried.

Rosin mildly-activating flux was applied with a swab to the recessed channel of the plated SS fixture and to the preforms. The preform is loaded into the holder, followed by the diamond substrate with the Au-plated side face down. The complete stack-up of the assembly is shown in Fig. 4a. The preform is slightly too large

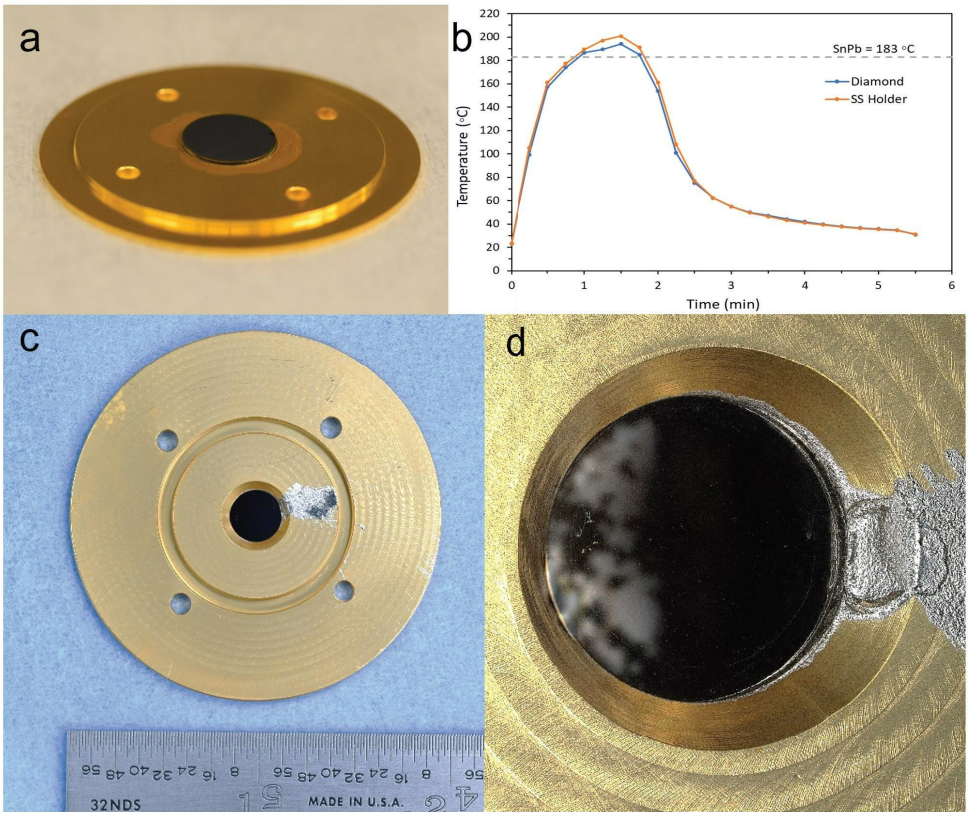

Figure 4. a) Stack of substrate over the solder preform loaded onto the plated SS anode holder, prior to solder reflow. b) Thermal Profile from the initial calibration run to determine solder reflow timing. c) Frontside of the soldered SS holder after ultrasonic cleaning. d) Close-up of frontside.

for the channel, so the stack-up is not flush prior to reflow. The stack is loaded onto a hotplate and once the solder is molten, a 10 g weight is stacked on top of the substrate to keep the sample flush and to eliminate voids. An initial thermal calibration run was performed on a test sample using thermocouples taped to the SS holder and the diamond substrate. All subsequent assemblies were reflowed on a hotplate approximately following the pre-determined thermal profile shown in Fig. 4b. Samples were removed from the hotplate after 2 minutes and cooled at room temperature. Samples were re-cleaned in an ultrasonic bath for 2 mins with Aerotron-100^{TM} and IPA. Cleaning with degreaser in the ultrasonic bath thoroughly removed the flux and eliminated residue build-up in the inner face of the substrate. Cracking was not visible in the substrate following sonication. An example of a fully soldered SS assembly post-cleaning is shown in Fig. 4c and d.

3.4.3 Helium Leak Testing

A standard helium (He) overspray test was performed on the soldered SS holders by attaching a Klein Flansche (KF, "quick release") vacuum flange. The testing apparatus underwent He leak testing to confirm the hardware was hermetic. This was done by applying a small bead of vacuum putty to a flat piece of metal, the "Blank", then performing an overspray test. In the same manner a thin bead of vacuum putty was applied to the bottom of the packaging holder to make a hermetic seal. Vacuum putty was also applied to the mounting thru holes on the SS holder to ensure no erroneous leak pathways were exposed during the test of the solder seal. Vacuum was applied by the helium leak detector to evacuate the space between the flange and the part under test; system pressure was approximately 26.2 mTorr during testing. Leak rates for all soldered holders measured to background levels of 5×10^{-10} atm-cc/sec He, as He was sprayed over the potential leak sites; data is shown in Fig. 5. All parts were confirmed to be hermetic.

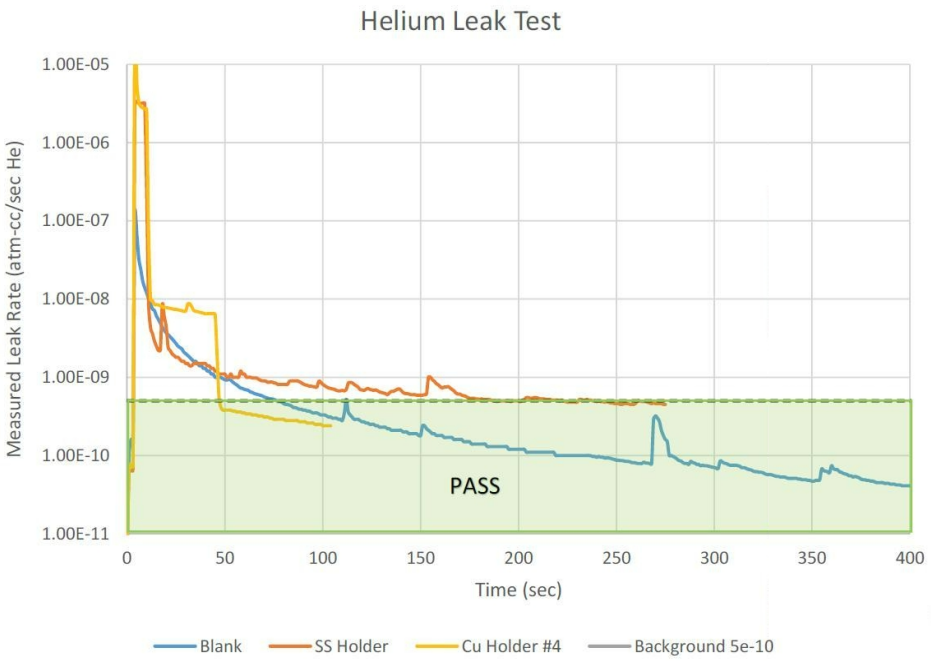

Figure 5. Example of measured leak rates for perimeter-plated diamond substrates soldered into a Cu fixture and SS fixture during helium overspray leak test.

4. FABRICATION

All fabrication of the anode metals was done in the MESA Microfab Class 100 Cleanroom at Sandia National Laboratories.

4.1 Reflection Anode

As described in the design of the reflection anodes, Sec. 3.2, the metal layers should preferentially be ordered from highest density at the base to lowest density at the surface. The most commonly available high energy reflection anodes, including the one used for our system at Sandia, have a solid W head. During operation in the X-ray tube, an ethylene glycol-based coolant is flowed through the open ports along the length of the anode's post. As we were depositing metals on a previously used anode, it was cleaned with a sequence of soaks in acetone, methanol, and IPA followed by wiping with IPA and drying with N_2 to remove any coolant residue prior to deposition. A custom mounting fixture was developed to allow plating of the W reflection anode in a standard Temescal electron-beam evaporation chamber. A thru-hole was added to the variable angle platen (VAP) for that chamber, slightly offset from the platen center to avoid striking the quartz crystal monitor of the chamber during operational rotation when mounted at an approximate angle of 30°. This was the steepest angle available to try and bring the slanted anode surface perpendicular to the evaporation source without making contact. Metal layers were deposited *in situ* to target 20 Å Ti, 5000 Å Ag, 20 Å Ti, 5000 Å Au at the VAP surface, with delays to allow time for cooling and pumping back down to lower vacuum levels in between as necessary to maintain the vacuum level $>10 \times 10^{-10}$ Torr. High-vacuum aluminum foil was wrapped around the majority of the anode post to avoid unnecessary metal deposition in the channels for the sealing gaskets along the length. An offset glass slide pair was mounted to the platen to serve as a deposition thickness monitor. It was expected that the deposition at the head of the reflection anode would be thicker than the platen surface as it was closer to the evaporation sources, but as we wanted effectively as thick as we could deposit, this was desirable. The chamber temperature reached approx. 55 °C by the end of the Au deposition, much cooler compared to the peak temperature of 273 °C observed during the previous Mo deposition that had failed. As shown in Fig. 6, the film

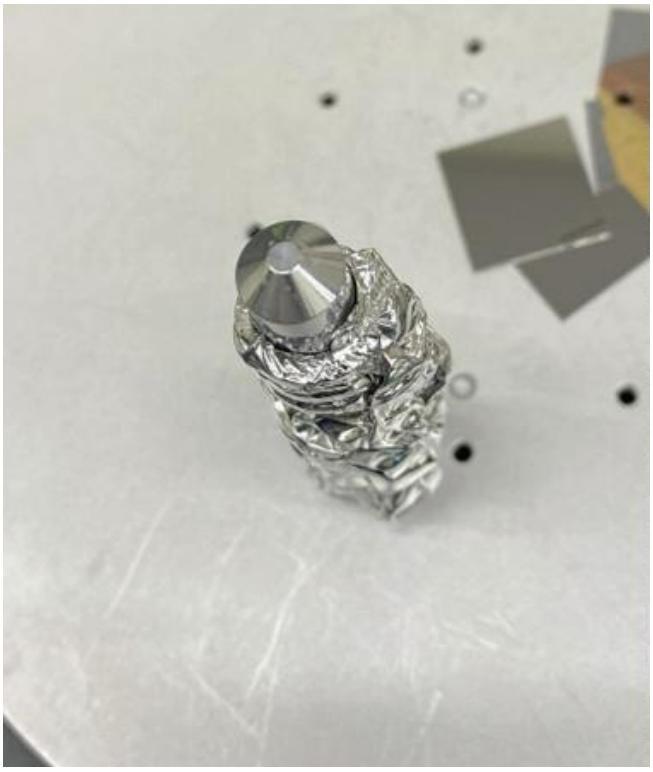

Figure 6. Photo of the reflection anode after 20 Å Ti, 5000 Å Au, 20 Å Ti, and 5000 Å Ag were deposited in a Temescal evaporator. The metal film is visually smooth.

quality was visually smooth upon removal from the chamber and did not experience delamination in the weeks following nor during X-ray tube operation.

4.2 Transmission Anodes

The transmission anodes were fabricated in two varieties: a bulk, layered metal stack and a patterned dot array. An overview of the patterned anode process flow is shown in Fig. 7. The anode fabrication was done in batches and included diamond substrate preparation, several rounds of photolithography-metal deposition-metal liftoff, and then photolithography around the substrate perimeter for electroplating. The layered anodes were fabricated alongside the patterned anodes but skipped all photolithography and metal liftoff steps besides those for the seed metal and electroplating. The NiAu electroplating of substrates and holders was outsourced within Albuquerque and is described alongside the packaging development in Sec. 3.4.2.

The diamond substrates were held by their perimeter with carbon fiber tweezers for all manipulation. Prior to processing they are rinsed with a sequence of acetone, methanol, and IPA and dried with a nitrogen (N_2) gun and then are exposed to a five-minute oxygen plasma in a barrel asher.

Two types of contact photolithography are done to pattern the diamond anodes between the five layer sequences. The first layer, the W sputtering, uses a dark field mask and positive photoresist (PR) bilayer while the subsequent photolithography layers for the three evaporations and final plating use bright field masks and negative PR. The key distinction is that with positive PR, the resist exposed to light is dissolved in the developer whereas for negative PR, the resist exposed to light is kept while the remainder is dissolved. A benefit of this is that negative resist tends to have a sloping undercut profile because the lower portion of the resist is less exposed than the surface. The shape and steepness of the undercut is tuned by resist and dose selection as well as develop duration. Conversely, positive PR is designed to achieve relatively vertical sidewalls.

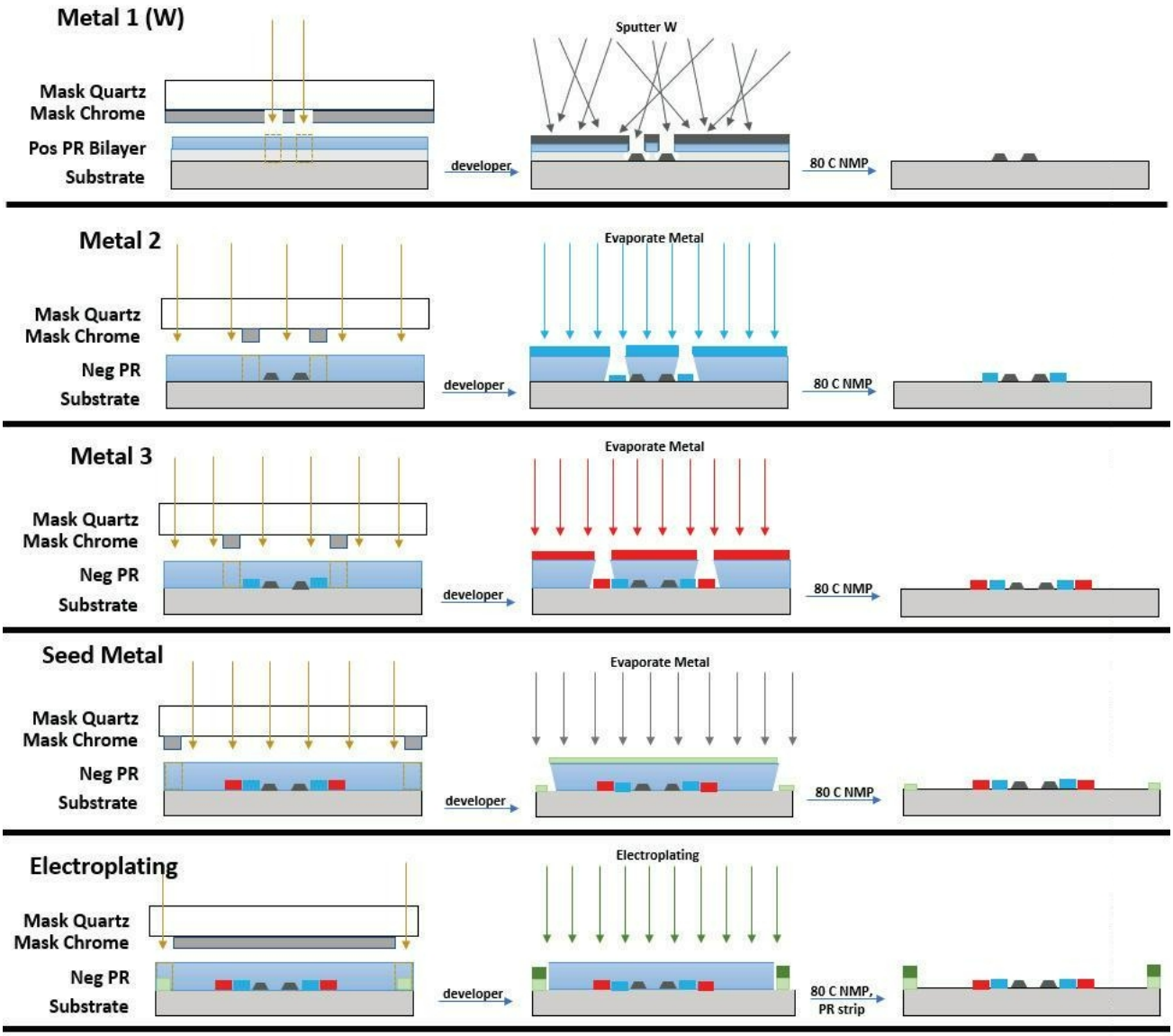

Figure 7. Schematic of the Patterned Anode process flow, visually demonstrating the multiple iterations of photolithography-metal deposition-metal liftoff.

A positive resist bilayer is used for the W patterning because sputtering is non-directional and tends to coat topography and sidewalls. This process, shown at the top of Fig. 7 makes use of a steeply undercutting bottom layer in the resist stack to avoid continuity from top unwanted metal and the metal in contact with the substrate that we want to keep. The LOR7a base layer in the stack, manufactured by Kayaku Advanced Materials, Inc., is not photo-sensitive and is dissolved away isotropically once the developer is through the top exposed resist. The LOR is spun to 0.7 µm thick to exceed the thickness of the 0.51 µm metal Ti/W stack being deposited. The top positive resist, UV210-0.3 by Rohm and Haas, is a deep-ultraviolet (DUV) resist that is exposed at a shorter wavelength of 270 nm compared to conventional photoresists exposed at 365 nm or 405 nm. It is used here for its thinness, around 0.3 µm, which helps to achieve smaller feature resolution. The negative resist, AZ nLOF 2020 by MicroChemicals, is used for the remaining evaporated-metal patterning. Negative resists are designed for liftoff of evaporated metal, among other things, by way of the undercut profile. Here the AZ nLOF 2020 is

spun to a thickness of 1.7 µm. The final photolithography process for electroplating is done with the same mask as for the evaporation of the seed metal and so still requires a negative resist. As electroplating conforms to the cavity, an undercut profile is not desired and is avoided by exposing the resist for longer. AZ nLOF 2035 was used in order to spin thicker, closer to 6.0 µm, to accommodate the thick 4 µm to 5 µm plating.

Prior to each metal deposition, samples are pre-cleaned in a 6:1 H_2O:BOE dip. BOE is a buffered oxide etch containing ammonium fluoride, hydrogen fluoride, and water. Samples patterned with nLOF photoresist are dipped for 20 sec while samples patterned with the LOR7a/UV210 positive photoresist bilayer are only dipped for 1 sec as the dilute BOE has been observed to damage the LOR. The BOE also roughens exposed Ag, so Layered substrates with exposed Ag surfaces are skipped and the rest are dipped for 20 sec.

For sputtering W, samples are loaded with clips to an aluminum platen. Offset glass slides and patterned silicon (Si) liftoff monitors are also clipped to the platen for thickness measurements. The platen is loaded face down into the load lock of the Kurt J. Lesker sputter chamber and the load lock is pumped down to reach a pressure $\leq 5 \times 10^{-6}$ Torr. The platen is transferred from the load lock into the process chamber and the chamber pressure is allowed to return to $<1 \times 10^{-7}$ Torr after the load lock door has closed. Ti is sputtered to a thickness of 100 Å followed *in situ* by 5000 Å of W using a quartz crystal monitor to measure the pre-rate and set the deposition durations. The chamber does not heat appreciably during the W sputtering. Once the deposition is complete, the platen is unloaded through the load lock and patterned samples proceed to metal liftoff. Layered samples proceed to the next metal deposition. All other candidate metals are deposited via evaporation in a Temescal BJD-1800 electron-beam evaporator. Samples are loaded with clips to aluminum platens. Offset glass slides and patterned Si liftoff monitors are also clipped to a platen for thickness measurements. The platens are loaded face down into a lift-off dome carousel. The metal source ingots or crucibles are loaded into their respective pockets in the chamber. The tool can have Au, Ti, Mo, and either Ag or Sm loaded simultaneously, among other metals not considered here. Once the metal sources and all samples are loaded, the chamber is pumped down to $\leq 7 \times 10^{-7}$ Torr.

The metals are deposited with only one candidate metal layer per run, as they need metal liftoff and then the next photolithography done in between. Each layer includes a thin 100 Å film of Ti deposited as an adhesion promoter, followed *in situ* by 5000 Å of the candidate metal (either Ag or Sm). The Sm was capped with a thin 100 Å of Au *in situ* to serve as an oxidation barrier. As described in Sec. 3.3.2, the layered transmission anodes must have their metal layers deposited in sequence from low density to high density. They are not patterned and could be deposited sequentially within one run in the Temescal with attention given to managing temperature and vacuum pressure in between layers. However, they were generally fabricated one layer at a time as they were run together with the patterned anodes for efficiency of tool time and material.

After metal deposition the patterned anodes are loaded vertically into a perforated parts basket and lowered into a beaker containing N-Methyl-2-Pyyrolidone (NMP) and a stir bar. The beaker is loaded onto a hotplate such that the stir bar is centered and then is heated to 75 °C to 80 °C while stirring at 100 rpm. The NMP dissolves the remaining photoresist out from under the unwanted metal and the metal is "lifted off". The parts are kept in the heated NMP for at least one hour and until the excess metal has cleared away from the substrate. Once the remaining photoresist is fully dissolved and the metal is cleared, the hot plate is turned off and the substrates are allowed to cool to room temperature within the NMP. They are then removed and rinsed with an IPA squirt bottle and are soaked in IPA for at least 5 minutes. They are rinsed with IPA again and then dried with N_2.

Once all candidate metals are deposited, the diamond substrates were pattern-seeded with 100 Å to 200 Å of evaporated Ti followed *in situ* by 2000 Å of evaporated Au and lifted-off. Substrates then had the final photoresist patterned to define the perimeter plating onto the patterned seed metal and were sent out to be electroplated with 4 µm to 5 µm Ni and 200 Å Au.

5. EVALUATION

CT measurements were collected on the bulk W reflection anode both before and after the custom layered metal deposition for comparison in emission spectra and presence of characteristic X-ray peaks. The X-ray tube used for these experiments was the X-RAY WorX XWT-225-SE, which can produce an electron beam with up to

225 keV accelerating voltage. This system is designed for reflection anodes only and as such only data from the custom-fabricated layered reflection anode was collected and compared against the commercial W reflection anode. The detector used was the Amptek 1-2-3 Cd-Te X-ray and Gamma Ray Spectrometer. The X-ray spectrometer was set to 1024 channels.

Emission spectra measurements were taken from 25 keV to 150 keV with increments of 25 keV. We did not go higher due to concern for the unknown longevity of the 0.5 µm metal films in the layered reflection anode when impinged upon by high-powered electrons. We used currents of 1, 5, 10, 15 and 20 µA at each voltage. The data was then normalized by dividing the number of counts in each channel by live-time of the detector for each measurement. This was done for both the original bulk W reflection anode and again after the Ti/Au and Ti/Ag candidate metal layers were added.

We also did an experiment to test the longevity of the metal films on the layered reflection anode. To do this we operated the layered reflection anode in our X-RAY WorX XWT-225-SE X-ray tube at 125 keV and 10 µA for five hours. Counts were averaged for 60 sec every 15 minutes during the 5 hours of continuous operation. The data was then normalized by live-time.

6. RESULTS

6.1 SEM Feature Characterization

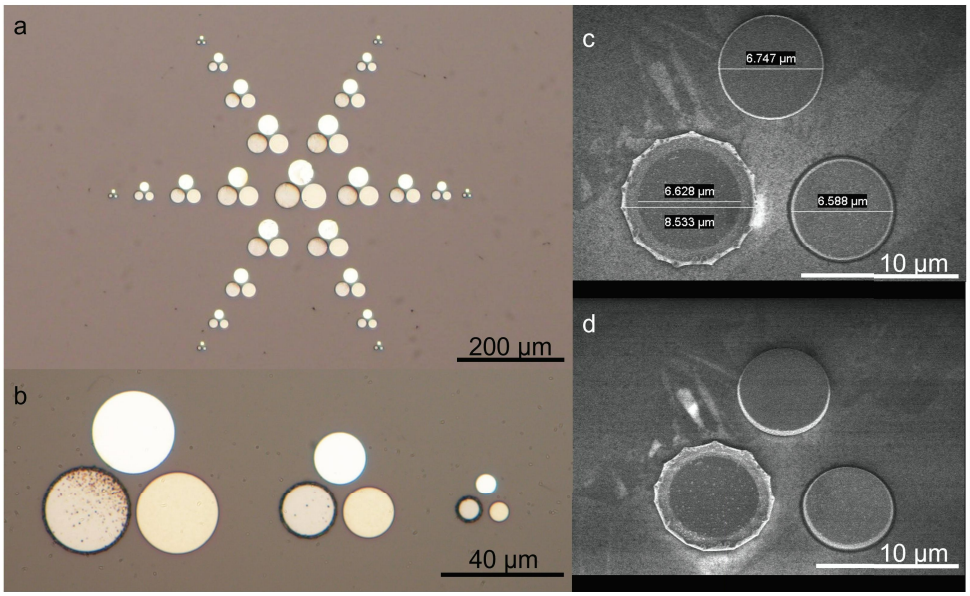

Figure 8. a) Optical image collected at 20x of the array of metal clusters patterned on a diamond substrate, scale bar is 200 µm. b) Optical image collected at 50x of one set of the three smallest cluster trios. The bottom left of each trio is sputter W, the top is evaporated Ag, and the bottom right is Au-capped Sm. Scale bar is 20 µm. c) SEM image of one of the smallest cluster trios, with the thin fringing around the W dot visible. d) SEM image of the same trio of dots, taken from a 30° tilt.

All films were characterized visually for film quality and smoothness using optical microscopes and scanning electron microscopy (SEM). Results from both are shown in Fig. 8. The roughness visible at the perimeter of the W dots is a consequence of poor liftoff of the sputter metal due to bridging from the top positive PR past the undercut to the metal being deposited on the substrate. There was some discontinuity or the bridge was sufficiently thin to still separate, but the thin fringe that remained increased the dot size by around 1 µm radially. The other two metals were evaporated rather than sputtered and lifted off cleanly. Fig. 8d is of the small cluster from a 30° angle and shows the difference in surface finish between the sputtered W and the two evaporated metals.

6.2 Emission Spectra

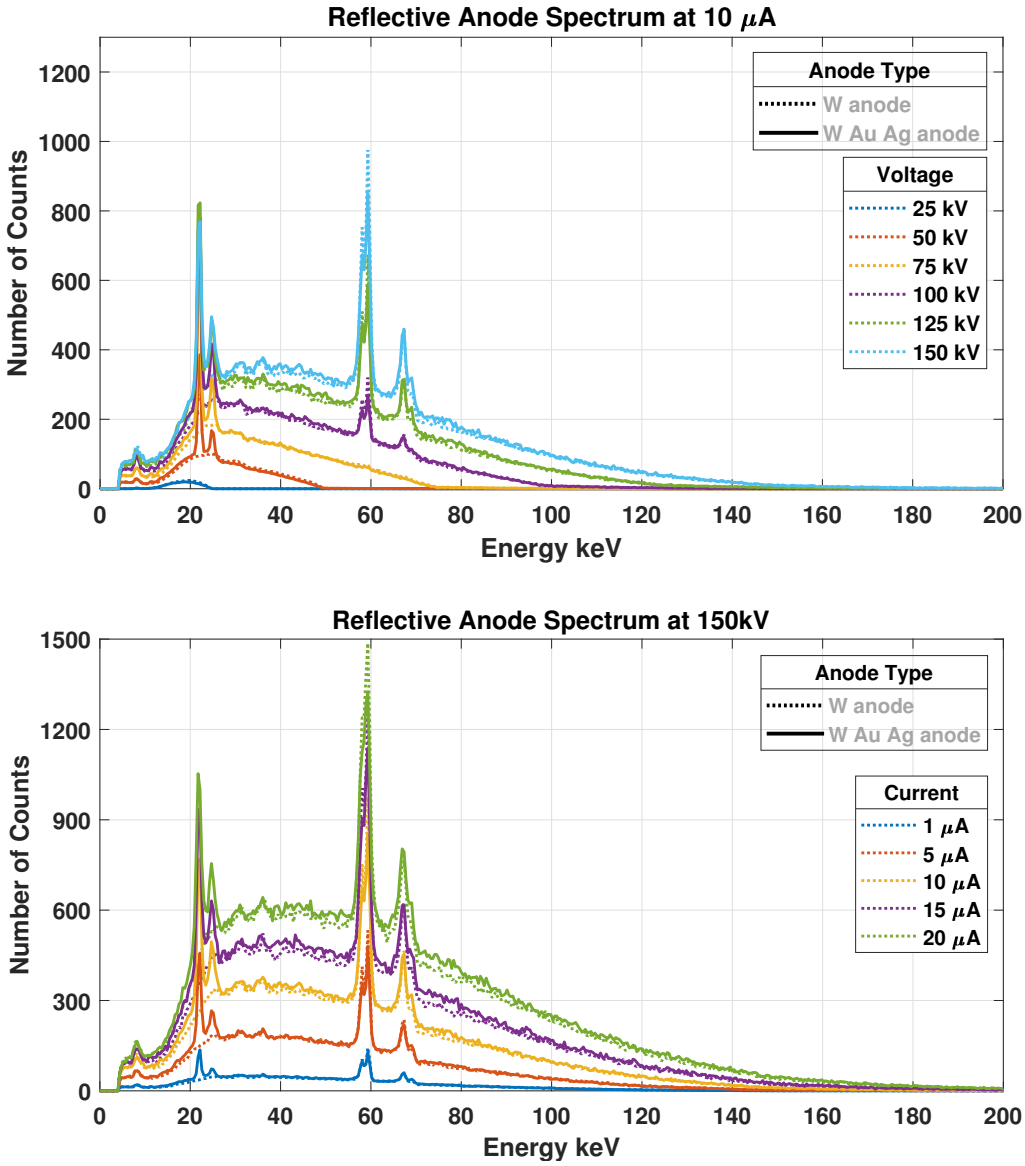

Figure 9. Measured spectral response of the reflection W anode with and without the Ti/Ag/Ti/Au metal layers added. Top) Spectral response at 10 µA electron beam current as accelerating voltage is varied from 25 keV to 150 keV. Bottom) Spectral response at 150 keV accelerating voltage as the electron beam current is varied from 1 µA to 20 µA.

Two sets of spectra from the reflected anode are shown in Fig. 9, with the upper plot showing the change in peak and background Bremsstrahlung radiation at an electron current of 10 µA as the accelerating voltage is varied from 25 keV to 150 keV. The lower plot shows the anode spectral response for a constant accelerating voltage of 150 keV with current varied from 1 µA to 20 µA. Subsets of the data are shown in Fig. 10 to emphasize the differences between the W and the layered reflection anode spectra with a strong presence of Ag peaks in the layered anode while no Ag peaks are present in the W anode. Also visible in Fig. 10 is a strong change in the Ag:W $K_{\alpha 1}$ peak ratio between 125 keV and 150 keV at 20 µA. Also clear in the subset plot, the main indication of the presence of Au in our layered anode is the small peak signal at the Au $K_{\alpha 1}$ in the layered anode compared

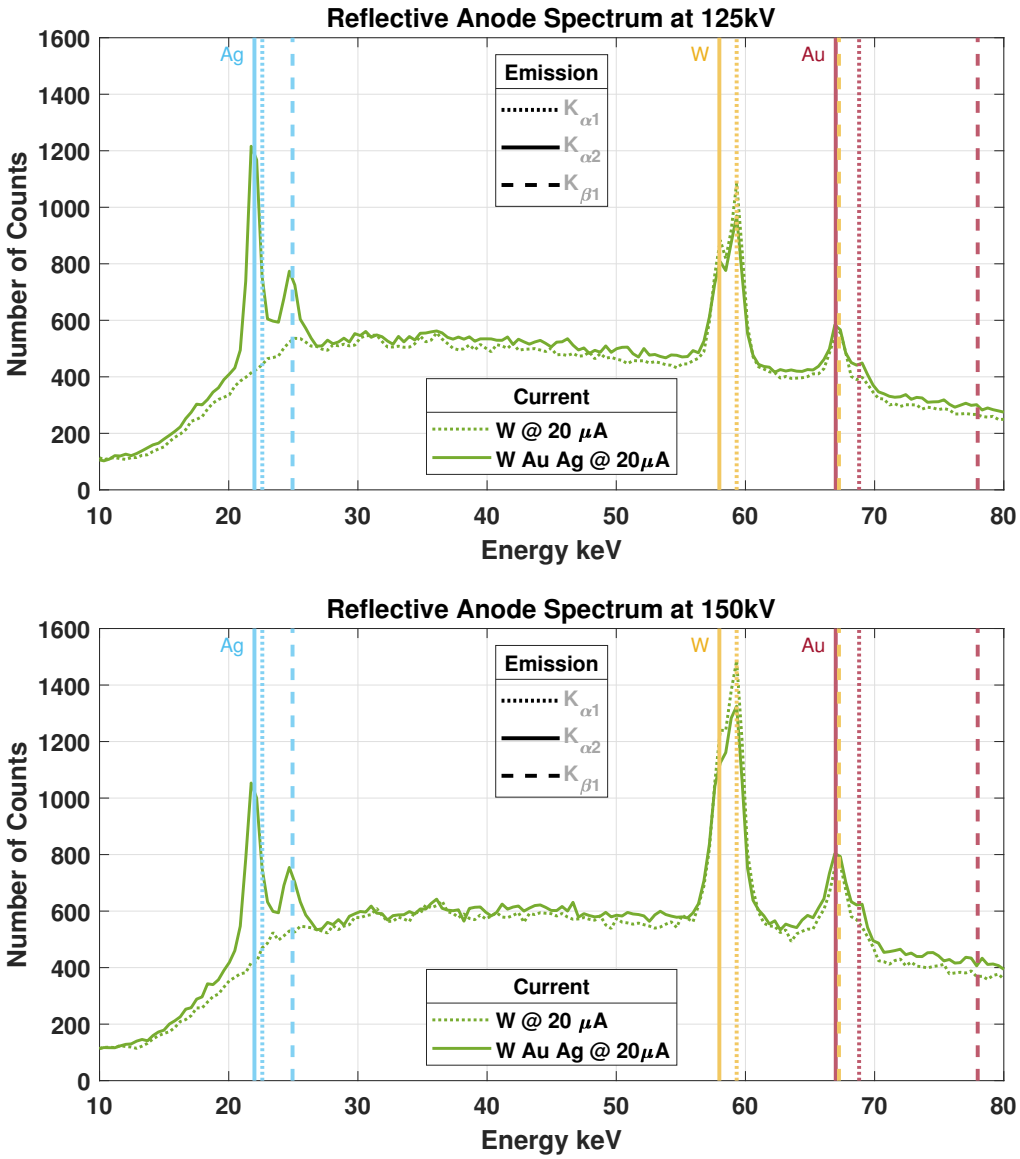

Figure 10. Subset of the measured spectral response shown in Fig. 9. Top) Spectral emission with an electron beam current of 20 µA and an accelerating voltage of 125 keV. Bottom) Spectral emission with a current of 20 µA and an accelerating voltage of 150 keV.

to the W anode.

There is a strong signal increase in the W and Au peak neighborhood and a decrease in the Ag K_α peak when the voltage is increased from 125 keV to 150 keV, indicating we may have reached an activation threshold for the W or Au at 150 keV.

6.3 Spectra Time Response

We also did an experiment to test for the time-dependent spectral response of the deposited metal films on the layered reflection anode. The results, shown in Fig. 11 as offset in counts measured from the mean, did not indicate any degradation in the number of counts in the channels corresponding to the Ag or W $K_{\alpha 1}$ peaks, nor a difference in the fluctuation of the Ag counts compared to the fluctuation of the W counts. This

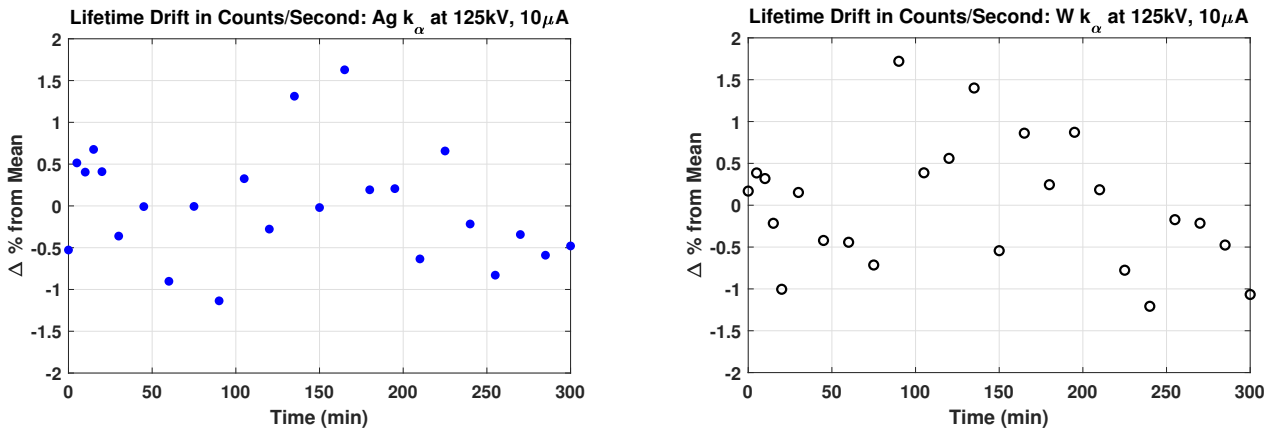

Figure 11. Measured counts in the channels corresponding to the Left) W and Right) Ag $K_{\alpha 1}$ characteristic peaks, relative to the respective mean channel count over 5 hours of continuous operation at 125 keV accelerating voltage and 10 µA electron current.

experiment indicates that the deposited 0.5 µm of Ag is thick enough to provide consistent X-ray generation during bombardment by high powered electrons for at least 5 hours. The Au emission signal was not extracted for this data set due to the relatively weak Au signal compared to the nearby W emission peaks.

7. CONCLUSION

We have successfully designed and fabricated custom patterned multi-metal transmission anodes with separate metals contained within the focal spot size of our commercial X-ray tube and smaller. We also fabricated bulk layered multi-metal transmission and reflection anodes for baseline quantification of emission spectra and longevity of the thin film anode materials. The custom fabricated transmission anodes were integrated successfully into custom-machined stainless steel packaging compatible with mounting to our existing commercial X-ray tubes and sources. The packaged custom transmission anodes were He-leak tested and the solder seals of the substrates to the holders were confirmed to be hermetic.

Initial X-ray CT measurements using our custom-layered reflection anode have demonstrated the added emission peaks for Ag and Au alongside the bulk W signal as well as material longevity of the deposited metal layers over extended X-ray tube operation. The inclusion of additional spectral neighborhoods of strong peak signal improves SNR in the emission spectra and enhances the ability to distinguish material composition of imaged samples.

8. FUTURE WORK

Following the success demonstrated by our custom layered reflection anode for material longevity as-fabricated, future work will include remeasuring the reflection anode with Ag/Au on bulk W with an aim to push the X-ray tube power higher both to access more of the high-energy photon generation, including Au, and to further test the custom-deposited metals' longevity under an increased power load.

Our group is also acquiring a new X-RAY WorX micro-focus dual-head X-ray source, XWT-225-XC, with interchangeable tube heads capable of mounting both transmission and reflection-style anodes. Our custom patterned and layered multi-metal transmission anodes will be characterized using this new source to compare emission spectra and time response as well as SNR and pixel response using the hyperspectral detector. Spatial resolution of the patterned anodes will also be characterized by measuring line-pair gauges for comparison against commercial bulk anodes as well as Dalton et al.'s[6] simulated results.

Further, additional candidate anode metals will be considered, simulated, and fabricated for generation of a broader range of spectral peaks and combinations. Performance of the various custom anodes will be compared

by imaging of multiple complex sample types such as low- and high-Z components together or soft materials. Performance will also be compared between the custom patterned multi-metal anodes using various detector configurations and materials.

ACKNOWLEDGMENTS

We would like to thank the SNL MESA metal tool engineers and technicians Steve Wolfley, Major Monochie, and Jeffrey Kronz for their assistance with the metal deposition development. We would also like to thank Ivan Gonzales Medellin and Monte Toledo of SNL's Rapid Prototyping Shop for assistance with our holder fabrication.

Sandia National Laboratories is a multi-mission laboratory managed and operated by the National Technology and Engineering Solutions of Sandia LLC, a wholly owned subsidiary of Honeywell International Inc. for the U.S. Department of Energy's National Nuclear Security Administration under contract DE-NA0003525. This paper describes objective technical results and analysis. Any subjective views or opinions that might be expressed in the paper do not necessarily represent the views of the U.S. Department of Energy or the United States Government.

REFERENCES

[1] Gallegos, I. O., Koundinyan, S., Suknot, A. N., Jimenez, E. S., Thompson, K. R., and Goodner, R. N., "Unsupervised learning methods to perform material identification tasks on spectral computed tomography data," in [*Radiation Detectors in Medicine, Industry, and National Security XIX*], Grim, G. P., Furenlid, L. R., and Barber, H. B., eds., *Proc. SPIE* **10763**, 107630G (2018).

[2] Jimenez, E. S., Collins, N. M., Holswade, E. A., Devonshire, M. L., and Thompson, K. R., "Developing imaging capabilities of multi-channel detectors comparable to traditional x-ray detector technology for industrial and security applications," in [*Radiation Detectors: Systems and Applications XVII*], Grim, G. P., Barber, H. B., and Furenlid, L. R., eds., *Proc. SPIE* **9969**, 99690A (2016).

[3] Jimenez, E. S., Thompson, K. R., Stohn, A. M., and Goodner, R. N., "Leveraging multi-channel x-ray detector technology to improve quality metrics for industrial and security applications.," in [*Developments in X-Ray Tomogaphy VIII*], Muller, B. and Wang, G., eds., *Proc. SPIE* **11840**, 118400H (2017).

[4] Zhou, R., Zhou, X., Li, X., Cai, Y., and Liu, F., "Study of the microfocus x-ray tube based on a point-like target used for micro-computed tomography," *PLoS ONE* **11(6)**, e0156224 (2016).

[5] Morimoto, N., Fujino, S., Yamakazi, A., Ito, Y., Hosoi, T., Wantanabe, H., and Takayoshi, S., "Two-dimensional x-ray phase imaging using single grating interferometer with embedded x-ray targets," *Optics Express* **23(13)**, 16582–16588 (2015).

[6] Dalton, G. M., Collins, N. M., Clifford, J. M., Kemp, E. L., Limpanukorn, B., and Jimenez, E. S., "Monte-carlo modeling and design of a high-resolution hyperspectral computed tomogaphy system with multi-material patterned anodes for material identification applications," in [*Developments in X-Ray Tomogaphy VIII*], Muller, B. and Wang, G., eds., *Proc. SPIE* **11840**, 118400H (2021).

[7] Devision, A. M. A., "Choosing the anode material in an X-ray tube." FAST ComTec GmbH https://www.fastcomtec.com/fwww/datashee/amptek/Choosing_the_anode_material.pdf. (Accessed: 28 September 2022).

[8] Thompson, A., Attwood, D., Gullikson, E., Howells, M., Kim, K., Kirz, J., Kortright, J., Lindau, I., Liu, Y., Pianetta, P., Robinson, A., Scofield, J., Underwood, J., Williams, G., and Winick, H., [*X-ray Data Booklet*], Lawrence Berkeley National Laboratories, Berkeley, CA (2009 (third edition)).

[9] Griesmann, U., "GDSII Toolbox." Ulf's Cyber Attic, 2016 https://sites.google.com/site/ulfgri/numerical/gdsii-toolbox. (Accessed: February 2017).